

An Efficient Algorithm for Density Functional Theory Simulation of Large Quantum Dot Systems

Hong Jiang,^{1,2,3} Harold U. Baranger,^{2,*} and Weitao Yang^{1,†}

¹Department of Chemistry, Duke University, Durham, North Carolina 27708-0354

²Department of Physics, Duke University, Durham, North Carolina 27708-0305

³College of Chemistry and Molecular Engineering, Peking University, Beijing, China 100871

(Dated: February 7, 2020)

Kohn-Sham spin-density functional theory provides an efficient and accurate model to study electron-electron interaction effects in quantum dots, but its application to large systems is a challenge. An efficient algorithm for the density-functional theory simulation of quantum dots is developed, which includes the particle-in-the-box representation of the Kohn-Sham orbitals, an efficient conjugate gradient method to directly minimize the total energy, a Fourier convolution approach for the calculation of the Hartree potential, and a simplified multi-grid technique to accelerate the convergence. The new algorithm is tested in a 2D model system. Using this new algorithm, numerical studies of large quantum dots with several hundred electrons become computationally affordable.

PACS numbers:

I. INTRODUCTION

Quantum dots (QD) are one kind of nano-device in which the motion of electrons is quantized in all three dimensions through the lateral confinement of a high-mobility modulation-doped two-dimensional electron gas in a semiconductor hetero-structure.^{1,2,3} Both quantum interference and electron-electron interactions play important roles, and their interplay underlies many properties that are fascinating in terms of both fundamental mesoscopic physics and future technical applications. Various theoretical models have been developed to explain experimental discoveries and to predict new properties. The Kohn-Sham (KS) density functional theory (DFT) method^{4,5,6} provides an accurate numerical model to study electron-electron interaction effects in QD systems.^{7,8,9,10,11,12,13,14,15,16,17,18} In spite of its comparatively low computational cost, previous DFT calculations are limited to systems in which the electron number is generally less than a few tens. In many experimental cases, however, the electron numbers involved are more than several hundred. The main theoretical approaches in the regime of large number of electrons are statistical methods^{2,3,19,20} which are usually based on some general assumptions whose validity, in many cases, is yet to be justified. It is therefore desirable to explore the large dot regime directly by using numerically more accurate models such as DFT. This imposes a demanding computational task because to obtain meaningful statistics, many calculations with several hundred electrons need to be done. It is therefore compelling to develop more efficient numerical techniques for DFT simulation of QD systems; this is the main object of the current study.

Two key issues are involved in the numerical implementation of the KS-DFT method:^{21,22} (1) the numerical representation of wave functions and the KS Hamiltonian, and (2) the solution of the numerical KS equation. While local basis sets (mainly Gaussian-type orbitals) dominate in conventional quantum chemistry of molecular systems, the plane wave (PW) basis,^{21,22} combined with the pseudo-potential method, is widely used in the *ab initio* electronic calculations of various material systems, in which the fast-Fourier trans-

form (FFT) method can be used to take full advantage of the periodicity of crystal structures. In principle, the PW method is valid only for periodic systems, but aperiodic systems can be treated by introducing the super-cell technique.²¹ In recent years, several groups have been advocating the use of basis-free real space methods for electronic structure calculations of finite systems, in which the wave functions are represented in real space, and the kinetic energy operator is discretized by a high-order finite difference (FD) method.²³ With a given representation, there are various methods to solve the resultant numerical KS equation. Roughly they fall into two different types: methods that minimize the total energy directly, and those that solve the KS equation in a self-consistent way. In addition, for DFT simulations of finite systems, another important issue is the calculation of the Hartree potential.

Aiming at modelling QD systems efficiently, we have developed new techniques in both the numerical representation of KS orbitals and the solution of the KS equation. We note that in QD systems, the wave functions vanish at the boundaries, and in some cases even the hard-wall boundary condition is used. For a function in a rectangular box with zero boundary values, the most natural basis set is the particle-in-the-box (PiB) basis set. The kinetic energy operator is diagonal in the PiB space and the transformation between real and PiB space can be efficiently performed by the fast sine-transform (FST) method, which is a variant of the FFT. For the solution of the KS equation, we modified Teter, Payne and Allan (TPA)'s band-by-band conjugate gradient method²⁴ to get a more efficient direct minimization approach.

The outline of the paper is as follows. In the next section, after a simple description of the KS-DFT method, we present the main components of our algorithm: (1) the PiB representation of the KS equation; (2) a modified band-by-band conjugate gradient method for the direct minimization of the KS total energy; (3) a Fourier convolution method for the calculation of the Hartree potential that was developed by Martyna and Tuckerman²⁵ in the PW pseudo-potential calculations; and (4) a simplified multi-grid technique to accelerate the convergence. In Section III, the new algorithm is tested in a 2D model QD system with electron number $N = 100$. Sec-

tion IV summarizes the main results and concludes the paper.

II. METHOD

A. Kohn-Sham spin-density-functional theory

Considering the important role played by electron spin in QD systems, we take the effect of spin polarization explicitly into account in the framework of Kohn-Sham spin-density functional theory (KS-SDFT).^{4,6} In KS-SDFT, the ground state energy of an interacting system with electron number N and the total spin S in the local external potential $V_{\text{ext}}(\mathbf{r})$ is written as a functional of spin densities n^σ with $\sigma = \alpha, \beta$ denoting spin-up and spin-down, respectively,

$$E[n^\alpha, n^\beta] = T_s[n^\alpha, n^\beta] + \int n(\mathbf{r})V_{\text{ext}}(\mathbf{r})d\mathbf{r} + \frac{1}{2} \int \frac{n(\mathbf{r})n(\mathbf{r}')}{|\mathbf{r} - \mathbf{r}'|} d\mathbf{r}d\mathbf{r}' + E_{\text{xc}}[n^\alpha, n^\beta]. \quad (1)$$

(Effective atomic units are used through the paper: for GaAs-AlGaAs QDs, the values are 10.08 meV for energy and 10.95 nm for length.) $T_s[n^\alpha, n^\beta]$ is the kinetic energy of the KS non-interacting reference system which has the same ground state spin density as the interacting one, and $E_{\text{xc}}[n^\alpha, n^\beta]$ is the exchange-correlation energy functional. The spin densities n^σ satisfy the constraint $\int n^\sigma(\mathbf{r})d\mathbf{r} = N^\sigma$ with $N^\alpha = (N + 2S)/2$ and $N^\beta = (N - 2S)/2$.

Assuming that the ground state of the non-interacting reference system is non-degenerate, the non-interacting kinetic energy is given by $T_s[n^\alpha, n^\beta] = \sum_{i,\sigma} \langle \psi_i^\sigma | -\frac{1}{2}\nabla^2 | \psi_i^\sigma \rangle$, and the ground state spin density is uniquely expressed as

$$n^\sigma(\mathbf{r}) = \sum_i^{N^\sigma} |\psi_i^\sigma(\mathbf{r})|^2, \quad \sigma = \alpha, \beta. \quad (2)$$

Here ψ_i^σ are the lowest single-particle orbitals which are obtained from

$$\mathbf{H}_{\text{KS}}^\sigma \psi_i^\sigma(\mathbf{r}) = \varepsilon_i^\sigma \psi_i^\sigma(\mathbf{r}), \quad (3)$$

with the KS Hamiltonian \mathbf{H}_{KS} defined as

$$\mathbf{H}_{\text{KS}}^\sigma \equiv -\frac{1}{2}\nabla^2 + V_{\text{ext}}(\mathbf{r}) + V_H[n; \mathbf{r}] + V_{\text{xc}}^\sigma[n^\alpha, n^\beta; \mathbf{r}]. \quad (4)$$

$V_H[n; \mathbf{r}]$ and $V_{\text{xc}}^\sigma[n^\alpha, n^\beta; \mathbf{r}]$ are the Hartree and exchange-correlation potentials, respectively,

$$V_H[n; \mathbf{r}] \equiv \int \frac{n(\mathbf{r}')}{|\mathbf{r} - \mathbf{r}'|} d^3\mathbf{r}', \quad (5)$$

$$V_{\text{xc}}^\sigma[n^\alpha, n^\beta; \mathbf{r}] \equiv \frac{\delta E_{\text{xc}}[n^\alpha, n^\beta]}{\delta n^\sigma(\mathbf{r})}. \quad (6)$$

We have used the local spin-density approximation (LSDA)^{4,6} for E_{xc} , which is widely used for the modelling of material systems. Although more accurate exchange-correlation functional forms such as the generalized-gradient

approximation (GGA) are available, it has been shown that the GGA results are close to those from LSDA calculations in QD systems.¹³ In terms of the implementation, the calculation of V_{xc} is trivial when the spin densities are in real space as is the case in our algorithm, but the calculation of V_H requires more efforts as will be shown later.

B. PiB Representation

To simplify the notation, we will take 1-D systems as an example, the generalization to higher dimensional cases being straightforward. Any regular function $f(x)$ that is localized in the finite region $0 < x < L$ with zero boundary values can be expanded as

$$f(x) = \sum_n C_n \sqrt{\frac{2}{L}} \sin \frac{n\pi x}{L} \quad (7)$$

and the expansion coefficients C_n are

$$C_n = \sqrt{\frac{2}{L}} \int_0^L f(x) \sin \frac{n\pi x}{L} dx. \quad (8)$$

Integrating Eq. (8) numerically on a set of equally spaced discrete points $\{x_j \equiv j\Delta x \equiv j\frac{L}{N_x}\}$ using the extended trapezoidal formula²⁶ leads to

$$C_n = \sqrt{\frac{2}{L}} \Delta x \sum_{j=1}^{N_x-1} f_j \sin \frac{\pi j n}{N_x} = F_n \frac{\sqrt{2L}}{N_x} \quad (9)$$

with $f_j \equiv f(x_j)$ and

$$F_n \equiv \sum_{j=1}^{N_x-1} f_j \sin \frac{\pi j n}{N_x} \equiv \mathbf{FST}\{f_j\} \quad (10)$$

where $\mathbf{FST}\{f_j\}$ denotes the fast sine-transform of the data $\{f_j\}$.

One of the key ingredients in our algorithm is the action of the single-particle Hamiltonian operator on wave functions,

$$\mathbf{H}f(x) = \mathbf{T}f(x) + \mathbf{V}f(x), \quad (11)$$

the efficiency of which is critical for the performance of the whole algorithm. Whereas the potential energy operator is diagonal in real space, the kinetic energy operator is diagonal in PiB space. Wave functions can be transformed between the two spaces efficiently by the fast sine transform. In our algorithm, wave functions are in discrete real space $\{f_j\}$, and the application of the potential energy operator is therefore trivial, $\mathbf{V}\{f_j\} = \{V_j f_j\}$, where V_j is the value of the potential at the point x_j . The kinetic energy operator is applied to wave functions in PiB space,

$$\mathbf{T}f(x) \equiv -\frac{\hbar^2}{2m} \nabla^2 f(x) = \frac{2}{N_x} \sum_n F_n \frac{\hbar^2 k_n^2}{2m} \sin \frac{n\pi x}{L}, \quad (12)$$

with $k_n = n\pi/L$, which in the discrete form becomes

$$\mathbf{T}\{f_j\} = \frac{2}{N_x} \mathbf{FST}\{F_n \frac{\hbar^2 k_n^2}{2m}\}. \quad (13)$$

The PiB representation formulated above is closely related to the PW method. In fact, for finite systems with soft-wall boundaries, the two representations are numerically equivalent. Mathematically, however, they are different: The PiB basis set is real and the zero boundary condition is imposed by the basis set itself, but in the PW case the basis functions are complex and the wave functions are forced to be zero at the boundaries by the external potential of systems under study. The PW method will fail in the case of the hard-wall boundary problem, which is quite common in the studies of quantum dots, but the PiB method is still valid.

C. Direct-minimization conjugate gradient method for the Kohn-Sham equation

In direct minimization approaches, the KS total energy functional is minimized directly over orbital wave functions under orthonormal constraints. We have made several important modifications to TPA's band-by-band conjugate-gradient scheme to obtain higher efficiency. Here we give an outline of the algorithm, and emphasize the modifications we have made.

The basic idea of a band-by-band scheme is to minimize the total energy over one band (or orbital) at a time, which, compared to other conjugate-gradient schemes,^{27,28} has the following advantages: (1) much lower requirement for storage space, (2) simpler implementation, and (3) particularly in our algorithm, an efficient approximate line-minimization scheme, as will be shown.

First the steepest descent (SD) vector for the i -th orbital at the m -th iteration is calculated from

$$|\zeta_i^m\rangle = \left(1 - \sum_{j \neq i} |\psi_j\rangle \langle \psi_j|\right) (\lambda_i^m - \mathbf{H}_{\text{KS}}) |\psi_i^m\rangle \quad (14)$$

with $\lambda_i^m = \langle \psi_i^m | \mathbf{H}_{\text{KS}} | \psi_i^m \rangle$ (to simplify the notation, we use Dirac's state vector notation and drop the spin index in the following formulation). In TPA's algorithm, the SD vector is preconditioned before it is used to build the conjugate vector. In our calculations, however, it was found that although in many cases preconditioning does accelerate the convergence, its effect is not always positive. On the other hand, the computational overhead in the preconditioning step, which involves another orthogonalization process as well as the action of the preconditioning operator on the SD vector, can be expensive for large systems. As shown later, by using a simplified multi-grid technique, we can achieve fast convergence even without preconditioning of the SD vectors.

The conjugate vector $|\varphi_i^m\rangle$ is then constructed as a linear combination of the SD vector $|\zeta_i^m\rangle$ and the previous conjugate vector,

$$|\varphi_i^m\rangle = |\zeta_i^m\rangle + \gamma_i^m |\varphi_i^{m-1}\rangle \quad (15)$$

where

$$\gamma_i^m = \frac{\langle \zeta_i^m | \zeta_i^m \rangle}{\langle \zeta_i^{m-1} | \zeta_i^{m-1} \rangle} \quad (16)$$

with $\gamma_i^1 = 0$. The conjugate vector is further orthogonalized to the present band $|\psi_i^m\rangle$ and normalized (\mathbf{N} is denoted as the normalization operator),

$$|\varphi_i^m\rangle = \mathbf{N} (1 - |\psi_i^m\rangle \langle \psi_i^m|) |\varphi_i^m\rangle \quad (17)$$

The new wave function for the i -th orbital $|\psi_i^{m+1}\rangle$ is formed from the linear combination

$$|\psi_i^{m+1}\rangle = |\psi_i^m\rangle \cos \theta_{\min} + |\varphi_i^m\rangle \sin \theta_{\min} \quad (18)$$

which is guaranteed to remain normalized and orthogonal to all other orbitals. θ_{\min} is obtained by minimizing the total energy as a function of θ with $|\psi_i(\theta)\rangle = |\psi_i^m\rangle \cos \theta + |\varphi_i^m\rangle \sin \theta$. In TPA's algorithm,^{21,24} θ_{\min} is determined by the following approximate scheme: The total energy as a function of θ is approximated by $E(\theta) \approx E_{\text{avg}} + A_1 \cos 2\theta + B_1 \sin 2\theta$; the three unknowns, E_{avg} , A_1 and B_1 , are determined according to three pieces of information: $E(\theta = 0)$, $\frac{\partial E(\theta)}{\partial \theta}|_{\theta=0}$ and $E(\theta = \pi/300)$.

Here we propose a more efficient approximate scheme for the determination of θ_{\min} . The derivative of $E(\theta)$ with respect to θ can be obtained from

$$\begin{aligned} \frac{\partial E(\theta)}{\partial \theta} &= 2 \langle \varphi_i^m | \mathbf{H}_{\text{KS}}(\theta) | \psi_i^m \rangle \cos 2\theta \\ &\quad - (\langle \psi_i^m | \mathbf{H}_{\text{KS}}(\theta) | \psi_i^m \rangle - \langle \varphi_i^m | \mathbf{H}_{\text{KS}}(\theta) | \varphi_i^m \rangle) \sin 2\theta \end{aligned} \quad (19)$$

Assuming $\mathbf{H}_{\text{KS}}(\theta) \approx \mathbf{H}_{\text{KS}}(0)$, from $\frac{\partial E(\theta)}{\partial \theta} = 0$ we get

$$\theta_{\min} = \frac{1}{2} \tan^{-1} \frac{B}{A} \quad (20)$$

with

$$A = -\langle \psi_i^m | \mathbf{H}_{\text{KS}}(0) | \psi_i^m \rangle + \langle \varphi_i^m | \mathbf{H}_{\text{KS}}(0) | \varphi_i^m \rangle \quad (21)$$

and

$$B = 2 \langle \varphi_i^m | \mathbf{H}_{\text{KS}}(0) | \psi_i^m \rangle. \quad (22)$$

The underlying approximation in our scheme is similar to that of TPA's, but our scheme is much more efficient in terms of computational effort: In TPA's scheme, at each band iteration the total energy must be calculated twice, i.e. $E(\theta = 0)$ and $E(\theta = \pi/300)$; in our scheme, the most time-consuming step is the action of \mathbf{H}_{KS} on $|\varphi_i^m\rangle$, which is much faster than the calculation of the total energy. Considering further the fact that the total number of band iterations can be very large, we note that an efficient line-minimization scheme such as ours is crucial to reduce the computational effort.

In TPA's algorithm, after the wave-function is updated according to Eq. (18), the Kohn-Sham Hamiltonian is updated immediately, which involves the reconstruction of $V_H(\mathbf{r})$ and

$V_{xc}(\mathbf{r})$ according to the new density. This is actually quite expensive for large systems. On the other hand, we expect that the KS Hamiltonian will not experience large changes inside the iterations of a single orbital. So in our algorithm, we update \mathbf{H}_{KS} after every N_{update} band iterations, and the optimal value of N_{update} will be explored in the next section.

In each orbital, the procedure described above is repeated N_{band} times; the iterations are then started on the next orbital. After the wave functions of all orbitals are updated in this way, the total energy is calculated and is compared to that of the previous cycle to determine if the final convergence is achieved. The main parameters in the algorithm are N_{band} and N_{update} . Their effects on the performance of the algorithm will be tested in detail in the next section.

D. Calculation of V_H

For finite systems, the simplest and perhaps most inefficient way to calculate V_H is by direct numerical integration, which is feasible only for small systems. Another widely-used approach is to solve the Poisson equation equivalent to Eq. (5). Though the Poisson equation itself can be solved with great efficiency, the calculation of boundary values can be quite expensive even by using efficient multipole expansion techniques. Additionally, the Poisson solver approach is valid only for 3D systems; in the case of 2D systems, there is no Poisson equation equivalent to Eq. (5). In recent years, several schemes have been proposed to extend the conventional Fourier convolution method to finite systems.^{25,29,30,31} In particular we have incorporated Martyna and Tuckerman's method²⁵ into our algorithm. Considering that the Martyna-Tuckerman method was developed mainly for the modelling of molecular and material systems within the plane-wave pseudo-potential framework, we will formulate the approach here with some detail.

The calculation of the Hartree potential is straightforward for periodic systems, but this is not the case for finite aperiodic systems. The potential $V_H(\mathbf{r})$ has the form of the convolution between the density and the Coulomb interaction kernel, $v_c(\mathbf{r}) = 1/r$, which has the following simple relation in the Fourier space,²⁶

$$\tilde{V}_H(\mathbf{k}) = \tilde{n}(\mathbf{k})\tilde{v}_c(\mathbf{k}), \quad (23)$$

where $\tilde{f}(\mathbf{k})$ refers to the Fourier transform of $f(\mathbf{r})$. Eq. (23) is useful only when we have the analytical form of $\tilde{n}(\mathbf{k})$ and can perform the inverse Fourier transform of $\tilde{V}_H(\mathbf{k})$ analytically, which is not true for most cases where the density is usually represented in discrete real space.

When applying the Fourier method to discrete finite systems, periodic boundary conditions are always assumed. It has long been known that the unphysical interactions between neighboring super-cells can be avoided by calculating V_H in a doubly extended grid.³² In particular for 2D systems as illustrated in Fig. 1, the original $L_x \times L_y$ grid (Ω) is extended to $2L_x \times 2L_y$ (Ω_{2L}). The density in the extended grid is defined

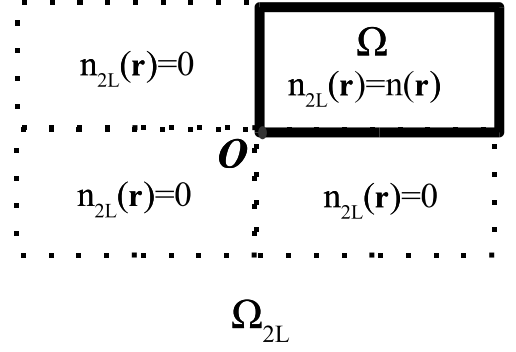


FIG. 1: Illustration of the Fourier convolution method for the calculation of the Hartree potential in finite systems. The original grid where the density and potential are defined is extended into doubled space. The density in the extended region is set to zero. Imposing the periodic boundary condition for this extended grid, the unphysical interaction between neighboring super-cells can be avoided.

as

$$n_{2L}(\mathbf{r}) = \begin{cases} n(\mathbf{r}) & \text{if } \mathbf{r} \in \Omega \\ 0 & \text{otherwise} \end{cases} \quad (24)$$

Imposing periodic boundary conditions to both the density and the Coulomb interaction kernel in the extended grid, the potential can be calculated according to the convolution theorem,

$$V_H(\mathbf{r}) = \sum_{\mathbf{k}} \bar{n}_{2L}(\mathbf{k}) \bar{v}_c(\mathbf{k}) e^{i\mathbf{k} \cdot \mathbf{r}} \quad (25)$$

where $\bar{n}_{2L}(\mathbf{k})$ and $\bar{v}_c(\mathbf{k})$ are respectively finite Fourier integrals of the density and the Coulomb interaction kernel in the extended grid,

$$\bar{n}_{2L}(\mathbf{k}) = \frac{1}{\Omega_{2L}} \int_{\Omega_{2L}} n_{2L}(\mathbf{r}) e^{-i\mathbf{k} \cdot \mathbf{r}} d\mathbf{r}, \quad (26)$$

$$\bar{v}_c(\mathbf{k}) = \int_{\Omega_{2L}} v_c(\mathbf{r}) e^{-i\mathbf{k} \cdot \mathbf{r}} d\mathbf{r} \quad (27)$$

where Ω_{2L} is used to denote both the extend grid and its volume (or area in the 2D case).

While $\bar{n}_{2L}(\mathbf{k})$ can be easily obtained from the discrete Fourier transform of its real space values by FFT, the calculation of $\bar{v}_c(\mathbf{k})$ is much more involved because of the singularity of the Coulomb interaction kernel in real space. The key to Martyna-Tuckerman's approach is to decompose the Coulomb interaction kernel into long- and short-range parts,

$$v_c(\mathbf{r}) = \frac{\text{erf}(\alpha r)}{r} + \frac{\text{erfc}(\alpha r)}{r} \equiv v_c^{(long)}(\mathbf{r}) + v_c^{(short)}(\mathbf{r}) \quad (28)$$

where $\text{erf}(x)$ and $\text{erfc}(x)$ are the error function and its complement, respectively, and α is the parameter that controls the effective cut-off range. The finite Fourier integral of the short range part can be well approximated by its infinite Fourier

transform,

$$\begin{aligned}\bar{v}_c^{(short)}(\mathbf{k}) &\equiv \int_{\Omega_{2L}} v_c^{(short)}(\mathbf{r}) e^{-i\mathbf{k}\cdot\mathbf{r}} d\mathbf{r} \\ &\approx \int_{\text{whole space}} v_c^{(short)}(\mathbf{r}) e^{-i\mathbf{k}\cdot\mathbf{r}} d\mathbf{r} \equiv \tilde{v}_c^{(short)}(\mathbf{k}).\end{aligned}\quad (29)$$

which is analytically known in both 2D and 3D cases. The finite Fourier integral of the long-range interaction can be directly obtained from the discrete Fourier transform of its real space values. In the practical implementation, \bar{v}_c needs to be calculated only once at the beginning. The calculation of $V_H(\mathbf{r})$ involves only two FFTs (one forward and one backward), which makes this approach much more efficient than methods based on a Poisson solver.

E. A simplified multi-grid technique

The multi-grid method is an efficient technique to accelerate the convergence in various real space relaxation approaches.²⁶ The basic idea is that low-frequency errors are easier to eliminate in a coarse grid than in a fine grid. Lee et al.³³ proposed a simple one-way multi-grid technique in finite-difference real space KS calculations. Wave functions being represented in real-space in our algorithm, a similar simplified multi-grid (SMG) method can be implemented in a straightforward way: the KS energy functional is first minimized in a coarse grid; the converged wave functions, after interpolation and re-orthogonalization, are taken as the initial guess for the minimization on the fine grid. With these well-preconditioned initial wave functions, the convergence in the fine grid can be easily attained.

III. NUMERICAL TESTS

In most experimental QD systems, the excitation in the vertical direction can be neglected, and a 2D model is a good approximation. In this paper we will report test results only in a 2D system; the extension to 3D systems is straightforward, and the high efficiency of our algorithm makes it possible to explore large dots even in the 3D case. We test the performance of the new algorithm in a coupled quartic oscillator potential system,

$$V_{\text{ext}}(\mathbf{r}) = a \left(\frac{x^4}{b} + by^4 - 2\lambda x^2 y^2 + \gamma(x^2 y - xy^2)r \right), \quad (30)$$

with $a = 10^{-4}$, $b = \pi/4$, $\lambda = 0.6$ and $\gamma = 0.1$. Considering that the convergence behavior in KS calculations is generally related to the effective interaction strength, which is characterized by $r_s \equiv (\pi\bar{n})^{-1/2}/a_B$ in the 2D case where \bar{n} is the average density and a_B is the Bohr radius, we have chosen the parameters in V_{ext} so that the estimated r_s is about 1.5, which is close to experimental values. The calculations are done in a grid of size $L_x = L_y = 50$ and the number of grid

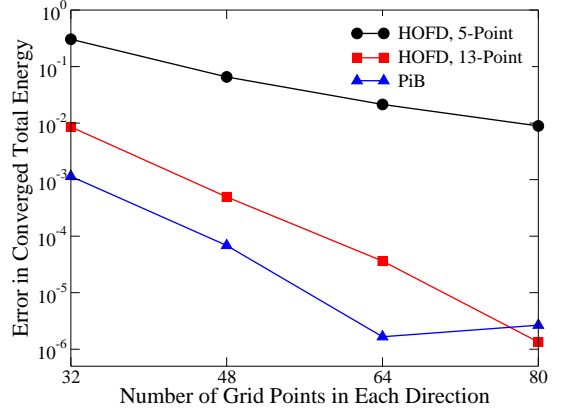


FIG. 2: Convergence of the total energy with respect to the number of grid points using 5-Point FD, 13-Point FD and PiB representation.

points is $N_x = N_y = 64$. All the following numerical results come from calculations with electron number $N = 100$ and spin $S = 0$. For the exchange-correlation energy, E_{xc} , we use Tanatar and Ceperley's parameterized form of the LSDA functional.³⁴ The convergence criterion is set as $\epsilon = 10^{-6}$, which corresponds to about 10^{-5} meV in GaAs-AlGaAs QD systems.

Considering that the FD method has been widely used in the numerical modelling of QD systems,^{7,8,13,16} we first make a comparison between FD and PiB. In the FD representation, the second order derivative in the kinetic energy operator is locally discretized in real space

$$\frac{\partial^2}{\partial x^2} f(x) = \frac{1}{h^2} \sum_{j=-m}^m C_j f_j + O(h^{2m}) \quad (31)$$

where h is the discretization step and the coefficients C_j can be obtained systematically for any m . Fig. 2 illustrates the convergence of the total energy with respect to the number of grid points using 5-point ($m = 2$), 13-point ($m = 6$) FD and PiB representations. The lower-order finite difference scheme, $m = 2$, is poor in terms of accuracy, and converges slowly as the grid size increases. The high-order FD scheme, $m = 6$, does improve the accuracy by two orders of magnitude, but is still less accurate than PiB for $N_x = 32, 48$ and 64 .

We check the accuracy and efficiency of our line-minimization scheme by comparing with TPA's approach as well as the numerically exact Brent's line search algorithm.²⁶ In this case, we use $N_{\text{band}} = 5$ and $N_{\text{update}} = 1$ as recommended in TPA's original algorithm.²¹ Fig. 3 plots θ_{\min} in the first 25 band iterations calculated from three schemes respectively. The values of θ_{\min} calculated from both TPA's and our method agree very well with exact values and the relative errors are always smaller than 1%. But in terms of computational effort, our new scheme is much more efficient as argued in the previous section.

To find the optimal N_{band} and N_{update} , we do the calculations with different values of N_{band} and N_{update} , and the results are shown in Fig. 4. With fixed $N_{\text{update}} = 1$, it is

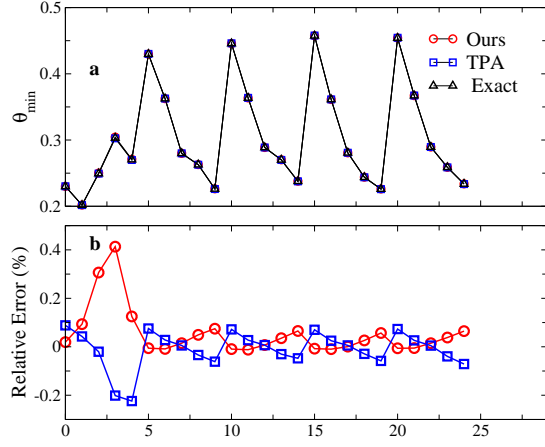


FIG. 3: Comparison of θ_{\min} calculated by three different schemes.

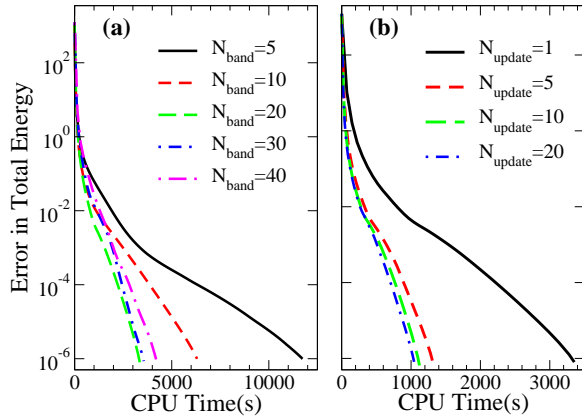


FIG. 4: Errors in the total energy as a function of CPU time during the DMCG calculation for different N_{band} with $N_{\text{update}} = 1$ (a) and for different N_{update} with $N_{\text{band}} = 20$ (b) with respect to the exact total energy that is calculated using a finer grid ($N_x = 80$) and tighter convergence criterion ($\epsilon = 10^{-7}$),

seen that a relatively larger N_{band} is more efficient than small N_{band} . Fixing $N_{\text{band}} = 20$, $N_{\text{update}} = 20$ gives the best performance. The combination of large N_{band} and N_{update} reduces the computational effort by almost one order of magnitude. Though the actual values of optimal N_{band} and N_{update} may vary for different systems, the basic idea demonstrated in this test calculation is believed to be of general significance.

We have implemented both the two-level (h and $2h$) and three-level ($h, \frac{4}{3}h$ and $2h$) SMG schemes. Instead of using a sophisticated interpolation as in Ref. 33, we use a simpler Lagrange polynomial interpolation method. Comparison with the single-level calculation shows a quite obvious improvement in computational efficiency. To check the effect of the interpolation accuracy, in Fig. 5 we plot the relative compu-

tational effort in one KS calculation as a function of the order of the Lagrange interpolation formula in both two- and three-level SMG calculations. We see that a high-order interpolation scheme is useful to improve the performance.

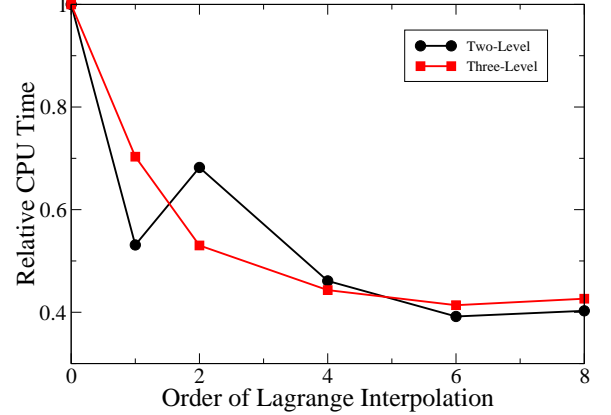


FIG. 5: Relative computational efforts for one KS calculation as a function of the order of interpolation in both two- and three-level SMG calculations. The CPU time in the single-level calculation is taken as the unit.

IV. SUMMARY

In this paper, we presented an efficient algorithm for the KS-SDFT simulation of large quantum dot systems. The main elements of the algorithm are: (1) Wave functions are represented in real space, and the kinetic energy operator is applied to wave functions by fast sine transform. (2) The Hartree potential is calculated by Martyna-Tuckerman's Fourier convolution method. (3) For the solution of the KS equation, we introduced several important modifications to Teter et al.'s band-by-band conjugate-gradient method. A more efficient approximate line-minimization scheme was developed; it was found that large band iteration number and a delayed update of the KS Hamiltonian inside the band iterations increase the efficiency by one order of magnitude. (4) A simplified multi-grid technique was introduced to accelerate the convergence. The new algorithm has been used to study spin and conductance peak-spacing distributions in a 2D chaotic QD system with electron number N up to 200, from which new physical phenomena were revealed.¹⁸

Acknowledgments

This work was supported in part by NSF Grant No. DMR-0103003.

* baranger@phy.duke.edu

† weitaoyang@duke.edu

¹ L. P. Kouwenhoven, C. M. Marcus, P. L. McEuen, S. Tarucha, R. M. Wetervelt, and N. S. Wingreen, in *Mesoscopic electron*

- transport, edited by L. L. Sohn, G. Schön, and L. P. Kouwenhoven (Kluwer, Dordrecht, 1997), pp. 105–214.
- ² Y. Alhassid, Rev. Mod. Phys. **72**, 895 (2000).
 - ³ I. L. Aleiner, P. W. Brouwer, and L. I. Glazman, Phys. Rep. **358**, 309 (2002).
 - ⁴ R. G. Parr and W. Yang, *Density-Functional Theory of Atoms and Molecules* (Oxford University Press, New York, 1989).
 - ⁵ R. O. Jones and O. Gunnarsson, Rev. Mod. Phys. **61**, 689 (1989).
 - ⁶ R. M. Dreizler and E. K. U. Gross, *Density Functional Theory : An Approach to the Quantum Many-Body Problem* (Springer-Verlag, Berlin, 1990).
 - ⁷ A. Kumar, S. E. Laux, and F. Stern, Phys. Rev. B **42**, 5166 (1990), 5166-5175.
 - ⁸ M. Macucci, K. Hess, and G. J. Iafrate, Phys. Rev. B **48**, 17354 (1993).
 - ⁹ D. Jovanovic and J. P. Leburton, Phys. Rev. B **49**, 7474 (1994).
 - ¹⁰ M. Stopa, Phys. Rev. B **54**, 13767 (1996).
 - ¹¹ S. Nagaraja, P. Matagne, V. Y. Thean, J. P. Leburton, Y. H. Kim, and R. M. Martin, Phys. Rev. B **56**, 15752 (1997).
 - ¹² M. Koskinen, M. Manninen, and S. M. Reimann, Phys. Rev. Lett. **79**, 1389 (1997).
 - ¹³ I.-H. Lee, V. Rao, R. M. Martin, and J.-P. Leburton, Phys. Rev. B **57**, 9035 (1998).
 - ¹⁴ S. Bednarek, B. Szafran, and J. Adamowski, Phys. Rev. B **64**, 195303 (2001).
 - ¹⁵ I. Yakimenko, A. M. Bychkov, and K.-F. Berggren, Phys. Rev. B **63**, 165309 (2001).
 - ¹⁶ M. Pi, A. Emperador, M. Barranco, and F. Garcias, Phys. Rev. B **63**, 115316 (2001).
 - ¹⁷ K. Hirose and N. S. Wingreen, Phys. Rev. B **65**, 193305 (2002).
 - ¹⁸ H. Jiang, H. U. Baranger, and W. Yang, Phys. Rev. Lett. (2002), accepted.
 - ¹⁹ D. Ullmo and H. U. Baranger, Phys. Rev. B **64**, 245324 (2001).
 - ²⁰ G. Usaj and H. U. Baranger, Phys. Rev. B **66**, 155333 (2002).
 - ²¹ M. C. Payne, M. P. Teter, D. C. Allan, T. A. Arias, and J. D. Joannopoulos, Rev. Mod. Phys. **64**, 1045 (1992).
 - ²² G. Kresse and J. Furthmüller, Phys. Rev. B **54**, 11169 (1996).
 - ²³ J. R. Chelikowsky, N. Troullier, K. Wu, and Y. Saad, Phys. Rev. B **50**, 11355 (1994).
 - ²⁴ M. P. Teter, M. C. Payne, and D. C. Allan, Phys. Rev. B **40**, 12255 (1989).
 - ²⁵ G. J. Martyna and M. E. Tuckerman, J. Chem. Phys. **110**, 2810 (1999).
 - ²⁶ W. H. Press, B. P. Flannery, S. A. Teukolsky, and W. T. Vetterlin, *Numerical Recipes: The Art of Scientific Computing* (Cambridge University, Cambridge, England, 1989).
 - ²⁷ I. Stich, R. Car, M. Parrinello, and S. Baroni, Phys. Rev. B **39**, 4997 (1989).
 - ²⁸ M. J. Gillan, J. Phys.:Condens. Matter **1**, 689 (1989).
 - ²⁹ G. Onida, L. Reining, R. W. Godby, R. Del Sole, and W. Andreoni, Phys. Rev. Lett. **75**, 818 (1995).
 - ³⁰ L. M. Fraser, W. M. C. Foulkes, G. Rajagopal, R. J. Needs, S. D. Kenny, and A. J. Williamson, Phys. Rev. B **53**, 1814 (1996).
 - ³¹ M. R. Jarvis, I. D. White, R. W. Godby, and M. C. Payne, Phys. Rev. B **56**, 14972 (1997).
 - ³² R. W. Hockney, Methods Comput. Phys. **9**, 135 (1970).
 - ³³ I.-H. Lee, Y.-H. Kim, and R. M. Martin, Phys. Rev. B **61**, 4397 (2000).
 - ³⁴ B. Tanatar and D. M. Ceperley, Phys. Rev. B **39**, 5005 (1989).